Peptides

International Edition: DOI: 10.1002/anie.201605203
German Edition: DOI: 10.1002/ange.201605203

Protonation-Driven Membrane Insertion of a pH-Low Insertion Peptide

*Samuel Z. Hanz[+], Nicolas S. Shu[+], Jieni Qian, Nathaniel Christman, Patrick Kranz, Ming An, Christof Grewer, and Wei Qiang**

Abstract: *The pH-low insertion peptide (pHLIP) inserts into membranes and forms a transmembrane (TM) α-helix in response to slight acidity, and has shown great potential for cancer diagnosis and treatment. As a lead, pHLIP is challenging to optimize because the mechanism of its pH-dependent membrane interactions is not completely understood. Within pHLIP there are multiple D/E residues which could sense the pH change, the particular role played by each of them in the protonation-driven insertion process is not clear. The precise location of the TM helix within the pHLIP sequence is also unknown. In this work, solid-state NMR spectroscopy is used to address these central questions. Tracing backbone conformations revealed that the TM helix spans from A10 to D33 with a break at T19 to P20. Residue-specific pK_a values of D31, D33, D25, and D14 were determined to be 6.5, 6.3, 6.1, and 5.8, respectively, and define the sequence of protonations which lead to insertion. Furthermore, possible intermediate states which disrupt membranes at pH 6.4 were proposed based on tryptophan fluorescence quenching and NMR data.*

The 36-residue (GGEQNPIYWARYADWLFTTPLLLLDLALLVDADEGT) pH-low insertion peptide (pHLIP), which is extracted from the bacteriorhodopsin helix C, can sense microenvironmental pH change and inserts into lipid bilayers as a transmembrane (TM) α-helix below a critical pH value.[1–6] The peptide is largely unfolded in aqueous solution (state I) and on the membrane surface (state II), and forms the folded state III upon insertion.[4] Biomedical applications of pHLIP (and its analogues) have attracted increasing attentions because of their controllable responses to slight acidity in the pH range of 6–7 found in various diseased states. They have been utilized as imaging tools and diagnostic agents for cancer, inflammation, and ischaemic myocardium.[1,4,5,7–10] Furthermore, pHLIP technology constitutes a new, pH-responsive, cross-membrane cytoplasmic cargo delivery platform. A variety of molecules, including fluorescent dyes, cytotoxins, chemotherapy drugs, and biomolecules, such as peptide nucleic acids (PNA), have been delivered into cells using pHLIP.[11–20] To extend the biomedical applications of pHLIP to broader systems with higher efficiency, appropriate tuning of its primary sequence is necessary,[21,22] and to do so requires an in-depth and detailed understanding of its pH-regulated membrane insertion process, which is currently not available.

The macroscopic, apparent pH_{50}, defined as the pH at which 50% of the pHLIP molecules are inserted (also referred to as p*K* or pK_a of insertion by others), has been estimated to be about 6.1–6.2 by following fluorescence changes of W residues at positions 9 and 15.[1,4] However, this assay is indirect and it is not clear which protonations of the D/E side chains within the pHLIP sequence correlate with a W fluorescence blue-shift and an increase of fluorescence intensity. The original hypothesis of how pH regulates pHLIP insertion rests on the notion that protonations of D residues in the TM domain of pHLIP increase the overall hydrophobicity of the peptide, ultimately leading to membrane insertion.[1] The central location of D14 and D25 residues make them likely to be in the TM region and protonations of their side chains were assumed to serve as the key triggering events for insertion.[1,5,21–23] Accordingly, modulation of pHLIP behavior has focused on modifying D14 and D25 side chains/ positions.[21,22,24] However, in addition to D14 and D25, there are two additional aspartic acid residues at positions 31 and 33. The roles played by D31 and D33 in pHLIP insertion have not been clearly defined,[6,23] partly because it unknown if D31/33 are in the TM helical region or not, because the residues which constitute the TM helix in the inserted state III have not been experimentally defined. In this work, we use solid-state nuclear magnetic resonance (ssNMR) spectroscopy to answer these critical questions in the protonation-driven membrane insertion of pHLIP.

With 1-palmitoyl-2-oleoyl-phosphatidylcholine (POPC) as the model membrane, we have previously shown that the structure of pHLIP in the inserted state III is well defined as α-helical at the selected residues from A10–A27, and consistent with earlier CD data.[25] Herein we fully characterize the secondary structures of pHLIP in the inserted state III (pH 5.3, pHLIP/ POPC ratio: 1:75). A representative two-dimensional (2D) ssNMR spectrum is shown in Figure 1 A, and the plot of secondary chemical shifts is shown in Figure 1 B. Additional spectra and a summary of ^{13}C chemical shifts are provided in the Supporting Information (see Figures S1–S3 and Table S1). There are several important conclusions that can be drawn from these NMR data: 1) The backbone α-helical conformation starts from A10 and ends at D33 and gives has a 36 Å span. 2) This helical span likely corresponds to the TM helix in state III because all D side chains, including the C-terminal D31 and 33, remain proton-

[*] S. Z. Hanz,[+] N. S. Shu,[+] J. Qian, N. Christman, P. Kranz, M. An, C. Grewer, Dr. W. Qiang
Department of Chemistry, Binghamton University
State University of New York
New York, NY 13902 (USA)
E-mail: wqiang@binghamton.edu
[+] These authors contributed equally to this work.

Supporting information for this article can be found under: http://dx.doi.org/10.1002/anie.201605203.

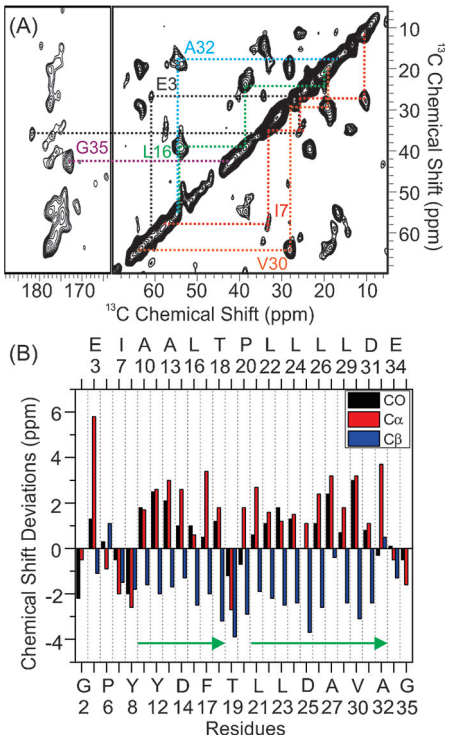

Figure 1. A) Two-dimensional ^{13}C-^{13}C spin diffusion spectra of pHLIP which was labeled with isotopes at E3, I7, L16, V30, A32, and G35. Intra-residue crosspeaks are shown with colored dashed lines. B) Plots of the residue-specific chemical shift deviation from random coils. The α-helical segments are highlighted with green arrows.

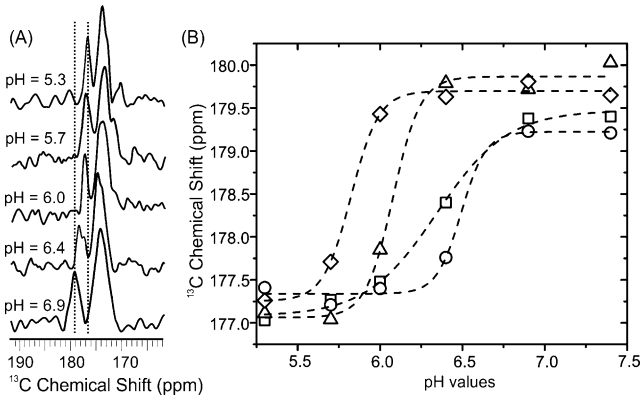

Figure 2. A) ^{13}C spectra for D33-labeled membrane-associated pHLIP at different pH values. The changes in the chemical shift of the side-chain carboxylic acid (Cγ) are highlighted using dashed lines. B) Plots of the Cγ chemical shifts versus pH values for individual aspartic acid residues (D33:squares; D31: circles; D25: triangles; D14: diamonds). Each data set was fitted to a sigmoidal function (shown in dashed curves) to determine the apparent pK_a value.

ated at pH 5.3 (the intrinsic D side chain pK_a in aqueous environment is ca. 3.9).[26] 3) Taken together with previous observations that A10 and A13 are located about 5.7 Å and 7.8 Å away from ^{31}P (assumed to be head groups of outer leaflet lipids) in state III,[25] it is very likely that the C-terminus of pHLIP is located in the phosphate head-group region of the inner leaflet of the bilayer because the ^{31}P-to-^{31}P thickness is about 38 Å for POPC and 38–43 Å for plasma membranes in mammalian cells. In other words, pHLIP is barely long enough to be truly transmembrane.[27] 4) A disruption to the backbone helix was observed at T19-P20, and is consistent with previous reported crystal structures of bacteriorhodopsin.[1–3] The non-helical T19-P20 may allow the TM span to be slightly longer. However, such flexibility is likely offset by the kink angle introduced by P20, as well as the overall tilt angle of TM pHLIP (15° from perpendicular).[1] The pHLIP-based drug delivery typically relies on selective intracellular cleavage of a disulfide linker which conjugates cargo to a C-terminal cysteine residue (usually second to last in a sequence).[21] The drug release efficiency may be improved when the primary sequence of pHLIP, especially the hydrophobic segment of L21-V30, is elongated, because then the TM α-helix may become longer and the disulfide linker may be more exposed to glutathione molecules in the cell.

Once the TM region of pHLIP was defined, studies were performed to understand the intermediate protonation states of pHLIP/POPC membrane interactions. The primary sequence of pHLIP contains six negatively charged D/E residues at physiological pH 7.4. Protonation of these residues increase the overall hydrophobicity, and has been proposed as the key factor for membrane insertion.[23,24] Analysis of backbone conformation and chemical shifts in state III suggests that all four aspartic acids, D14, D25, D31, and D33, are located within the TM helical region. Protonation of a D side-chain carboxylate induces a significant Cγ upfield shift which can be monitored by ssNMR spectroscopy.[26] Figure 2A shows the double-quantum-filtered (DQF) cross-polarization ssNMR spectra of membrane-associated pHLIP, ^{13}C-labeled only at D33, at several different pH values ranging from 7.4 to 5.3. The DQF was applied to remove the natural abundance carbonyl signal from lipids.[28] Additional spectra for D14, D25, and D31 are provided in Figures S4–S6. Plots of ^{13}C chemical shifts versus pH values shown in Figure 2B reveal that D31 has a pK_a value of 6.49 ± 0.07, followed by D33 with a pK_a value of 6.34 ± 0.21, D25 with pK_a of 6.08 ± 0.08, and D14 with pK_a of 5.82 ± 0.08. We were surprised to learn that the C-terminal D31 and D33 residues are protonated first during insertion. Since the C-terminal half of pHLIP (L21 to T36) contains mainly hydrophobic and D/E residues, protonations of D31 and D33 residues would dramatically reduce the hydrophilicity of the C-terminal region, thus allowing pHLIP to sink deeper into the membrane (pH 7.4 state II to pH 6.4 state II′ transition),[25] and in turn lead to subsequent D25 and D14 protonations and ultimately membrane insertion. All the detected pK_a values are considerably higher than the D side chain pK_a value of 3.86 in aqueous environments.[26] Thus, the protonated states are stabilized by the hydrophobic environment of the membrane and/or inter-residues interactions in pHLIP. Additionally, the slope of the pK_a titration curve for D33 is qualitatively different from those of D14, D25, and D31, thus suggesting that this residue may experience unique environmental changes upon pH variation from 7.4 to 5.3.

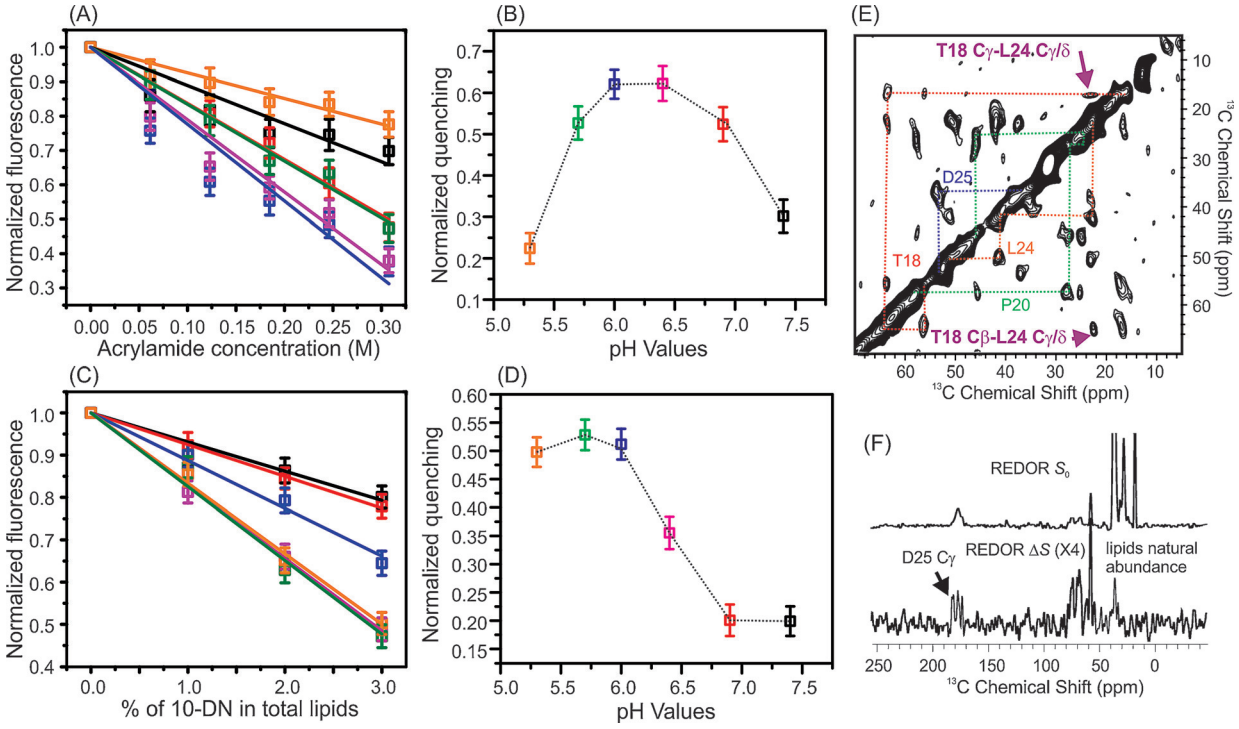

Figure 3. Plots of fluorescence quenching with (A-B) water-soluble acrylamide (A and B) and hydrophobic 10-DN (C and D). Samples with different pH values were color-coded: black, 7.4; red, 6.9; blue, 6.4; magenta, 6.0; green, 5.7, and orange, 5.3. Data in A and C show the normalized fluorescence versus concentrations of the quenching agents. Data in B and D show the normalized quenching versus pH at the maximum concentrations of quenching agents [0.3 M acrylamide for (B) and 3.0% 10-DN for (D)]. E) 2D spin diffusion ssNMR spectrum at pH 6.4 for pHLIP labeled at T18, P20, L24, and D25. Intra-residue crosspeaks are highlighted with dashed lines, and the inter-residue crosspeaks are indicated with purple arrows. F) ^{13}C-^{31}P REDOR S_0 and ΔS spectra at pH 6.4.

Next, quenching of tryptophan fluorescence was studied at different pH values using the POPC membrane. Two types of quenching agents, the water-soluble acrylamide and the lipid-like 10-doxyl-nonadacane (10-DN), were utilized.[4,29,30] Figures 3 A–D show tryptophan quenching by acrylamide or 10-DN, thus indicating the exposure of W side chains to water or hydrophobic membrane interior, respectively.[30] There are two tryptophan residues in pHLIP, W9 and W15. We learned previously from ssNMR data that at both pH 7.4 (state II) and 5.3 (state III): a) the β-carbon atom of A10 and A13 are located about 5.7 Å and 7.6–7.8 Å, respectively, away from head-group ^{31}P nuclei; and b) A13 has contacts with lipid alkyl chains.[25] Therefore, we expect W9 to be near the head-group phosphate level (or slightly above) and W15 below the head-group/ alkyl chain interface. Such membrane positions may lead to preferential quenching of the more exposed W9 by the aqueous phase quencher acrylamide, and the more deeply buried W15 by the lipid phase quencher 10-DN. The acrylamide/W9 pairing is also consistent with earlier published fluorescence decomposition study showing only one of the two W residues is accessible to acrylamide in state II. In our experiments, at pH 7.4 (state II),[4] the quenching level was moderate for either acrylamide (ca. 30% quenching at 0.3 M acrylamide) or 10-DN (ca. 20% quenching at 3.0% 10-DN in POPC). At pH 5.3 (state III), acrylamide quenching decreased from about 30 to 22% while 10-DN quenching increased from about 20 to 50% (Figures 3 B and D), thus suggesting that W9 is less exposed to water while W15 is closer to membrane center in inserted state III than adsorbed state II, and is consistent with the pHLIP insertion model and previous findings.[4,30]

The novel and more intriguing quenching data were obtained at intermediate pH values. For 10-DN, the quenching level increased with acidification, thus reaching a maximum as early as pH 6.0 (Figures 3 C and D). For acrylamide, instead of a corresponding gradual decrease in quenching as one might expect, a surprising and significant increase in quenching (about 30 to 50%) was observed even from pH 7.4 to 6.9, reaching the plateau of approximately 63% in the range of pH 6.4–6.0, and then decreasing dramatically after pH 5.7 (ca. 53%) and 5.3 (ca. 22%; Figure 3 B). We suggest that increased quenching by both acrylamide and 10-DN at the intermediate pH values reflect a chaotic membrane environment in which some water molecules intermingle with lipids. Such pHLIP-induced membrane disturbance is most prominent at pH 6.0–6.4. This hypothesis is also supported by our published ^{31}P T_2 relaxation measurements,[25] where the relaxation rates followed the trend of pH 6.4 < pH 7.4 < pH 5.3. The slower ^{31}P relaxation indicates a more dynamic lipid head group environment at pH 6.4 than at either pH 7.4 or 5.3.[31,32] Accordingly, the dramatic decrease in acrylamide quenching from pH 6.0 to 5.3 may signal the return of a chaotic deformed membrane to an orderly lipid bilayer after all the pHLIP molecules have inserted. The level of acryl-

amide quenching is lower at pH 5.3 than at 7.4, and consistent with previous conclusions that pHLIP disturbs more lipids in the adsorbed state II than inserted state III.[5,33]

It is interesting to consider the physical meaning of pHLIP pH_{50} of about 6.2 on a POPC membrane (aka overall pK or pK_a of insertion) in light of the new quenching data at intermediate pH values. The pH_{50} is usually determined by measuring the blue-shift of the tryptophan fluorescence λ_{max} in response to decreasing pH values.[4,34] At pH_{50} where the sigmoidal plot of λ_{max} versus pH is the steepest, changes in local environments around W residues are most dramatic, and the blue-shift was thought to reflect transition to more nonpolar surroundings, as a result from insertion of pHLIP into the membrane. As discussed above, our previous ssNMR data suggest that W9 and W15 residues are located near and below the interface between head groups and alkyl chains, respectively, over a broad pH ranging from 7.4 to 5.3. Acidification may sink W9 and W15 by about 2–3 Å, but the change might not be dramatic. Since a pH_{50} of about 6.2 is in the middle of the range where acrylamide quenching plateaued (pH 6.0–6.4), we wondered if the W fluorescence blue-shift could be partly induced by change in water accessibility. Contrary to general belief, it is known that a λ_{max} blue-shift could be caused by contacts between the indole ring and a small number of H_2O molecules in certain orientations, even when the W residue is situated in a generally hydrophobic environment.[35]

The pH_{50} of 6.21 ± 0.06[25] is between the pK_a value for D25 (6.08 ± 0.08) and those of D33 (6.34 ± 0.21) and D31 (6.49 ± 0.07). The increase in acrylamide quenching (and implied membrane disturbance) reached a maximum at pH 6.4 (Figure 3B), which coincides with protonation of D31 and sinking of pHLIP from the adsorbed state II (at pH 7.4) to the distinct and more deeply embedded (but still peripheral) state II′ (at pH 6.4, proposed based on our previous ssNMR data).[25] It seems reasonable to expect such a deeply embedded pHLIP would disrupt at least the outer leaflet of the lipid bilayer, and may facilitate subsequent TM insertion. Previous work from us and others showed that chemical modifications of D25 and D14 have significant effects on the pH_{50} value of pHLIP.[21,22] Thus, protonations of D14/25 may induce further structural and/or membrane location/interaction changes which allow pHLIP insertion to begin. Furthermore, the D14 pK_a of 5.82 ± 0.08 revealed the limitation of the λ_{max} blue-shift based a pH_{50} assay, as D14 protonation occurs over a pH range below the pH_{50} but coincides with dramatic decrease in acrylamide quenching, and signals the return to ordered bilayer. These crucial final events of pHLIP insertion do not seem to change the W fluorescence λ_{max} very much and thus they are invisible in the blue-shift assay. Future optimization of pHLIP sequence should not only focus on D14/25 but also D31/33, as all D residues may play distinct and critical roles in the protonation-driven membrane insertion process. To better understand variant behavior, the acrylamide quenching assay should be used along side the established tryptophan fluorescence blue-shift assay.

To investigate whether certain intermediate pHLIP structures are associated with the proposed membrane disturbance, we performed additional ssNMR measurements at pH 6.4. Figure 3E shows the long-range 2D spin diffusion spectrum for detecting the internuclear interactions within about 7 Å.[36,37] First, at pH 6.4, the Cα/Cβ chemical shifts of T18 ($\delta = 56.3$ ppm/ 63.8 ppm) and L24 ($\delta = 51.5$ ppm/ 42.1 ppm) are significantly different from those at pH 5.3 state III (T18: $\delta = 62.3$ ppm/ 64.7 ppm, L24: 54.9 ppm/ 38.3 ppm), thus indicating that these two residues are more likely to adopt non-helical conformations at pH 6.4, and gives this segment flexibility. This data also suggests that the helical population at pH 6.4 is different from that of state III at pH 5.3. Secondly, inter-residue crosspeaks were detected between T18 Cβ/Cγ and L24 Cγ/Cδ, thus suggesting that their side chains are in close proximity. We propose that the backbone kink around P20, which is seen in inserted pHLIP at pH 7.4, may be already present (and possibly more severe) at pH 6.4, with potential functional significance in membrane disruption/insertion by serving as a wedge. Previous 2D measurements at pH 6.4 demonstrated that residues L21, L22, L26, and A27 adopted one predominant set of chemical shifts, all with helical signatures, while residues A10 and A13 had two distinct sets of chemical shifts, one helical and one not-helical.[25] These two populations seem to interconvert on a time scale slower than a few milliseconds at 5–10 °C (so the chemical shift differences could be detected). The residue-specific pK_a data published here would describe two populations at pH 6.4 according to protonation states (Figure 2B), as "D31/33-doubly-protonated" (ca. 40%) and "only-D31-protonated" (ca. 60%) pHLIP intermediates. We suggest that the D31/33-doubly-protonated population is helical at pH 6.4 while the major only-D31-protonated population is not. Previously published CD measurements,[25] which showed that the level of helicity at pH 6.4 is only about 20–30% of that reached at pH 5.3 state III, support the notion that the major population at pH 6.4 is not helical. Figure 3F shows the ^{13}C-^{31}P rotational-echo double-resonance (REDOR)[25] spectra for the same sample used in probing T18/ L24 proximity, in which the close contact between D25 Cγ and head group ^{31}P can be identified. We have previously shown that A27 Cβ at pH 6.4 also had close contact to ^{31}P.[25] Therefore, the helical segment encompassing D25 and A27 is embedded in the phosphate head-group region with both side chains likely aligned parallel to the bilayer surface, and is consistent with previous stop-flow kinetic data showing that a peripheral helix is formed prior to pHLIP insertion.[11] The more helical, presumably D33-protonated pHLIP intermediate would have a different shape and volume than the non-helical (or less-helical), D33-deprotonated population. The interconversion between them (and the associated change in membrane location) may "mechanically" stir the lipids in a dynamic fashion with D33 protonation/ deprotonation equilibrium serving as the "motor". Membrane disorder at the interface of pHLIP and lipids seem inevitable as one considers the flickering helical content of pHLIP at pH 6.4.

Lastly, molecular dynamic (MD) simulations were performed on pHLIP in aqueous solution to investigate the residue-specific propensity for α-helical conformation, as well as the relationship between protonation and α-helix formation (see Figures S8–S10). When D/E side chains were deprotonated, MD simulations of up to 2 μs showed that

Y12–F17 and D25–E34 segments have high tendency to form an α-helix, while L21-L23 residues prefer to form a short 3^{10} helical turn (see Figures S8 and S9). However, the C-terminal α-helix (D25–E34) seems to be highly dynamic, and disappears/unfolds on the microesecond timescale (see Figure S9). When D/E residues were protonated in simulations, the C-terminal D25–E34 α-helix was stabilized, and then it expanded to include residues L21–L24, while the Y12–F17 α-helix also expanded towards the N-terminal region (Figure S10). After 2 μs of simulation, the final overall helical contents of D/E protonated pHLIP are remarkably consistent with the pH 5.3 state III NMR backbone data (see Table S1). Furthermore, the overall simulation data support the D33-protonation-driven α-helix formation hypothesis discussed for intermediates at pH 6.4. Lack of helical conformation around T19-P20 was observed throughout the simulations, and is also consistent with NMR data. Strikingly, simulated L24 residue also showed lower propensity for α-helix when compared to its leucine neighbors, and agrees well with NMR data at pH 6.4. Furthermore, the simulated Y12–F17 α-helix was stabilized by a potential salt bridge between the side chains of R11 and D14. In the presence of a membrane, R11 may preferentially bind to the negatively charged lipid head-group phosphates,[23] and consequently this helical conformation may be destabilized.

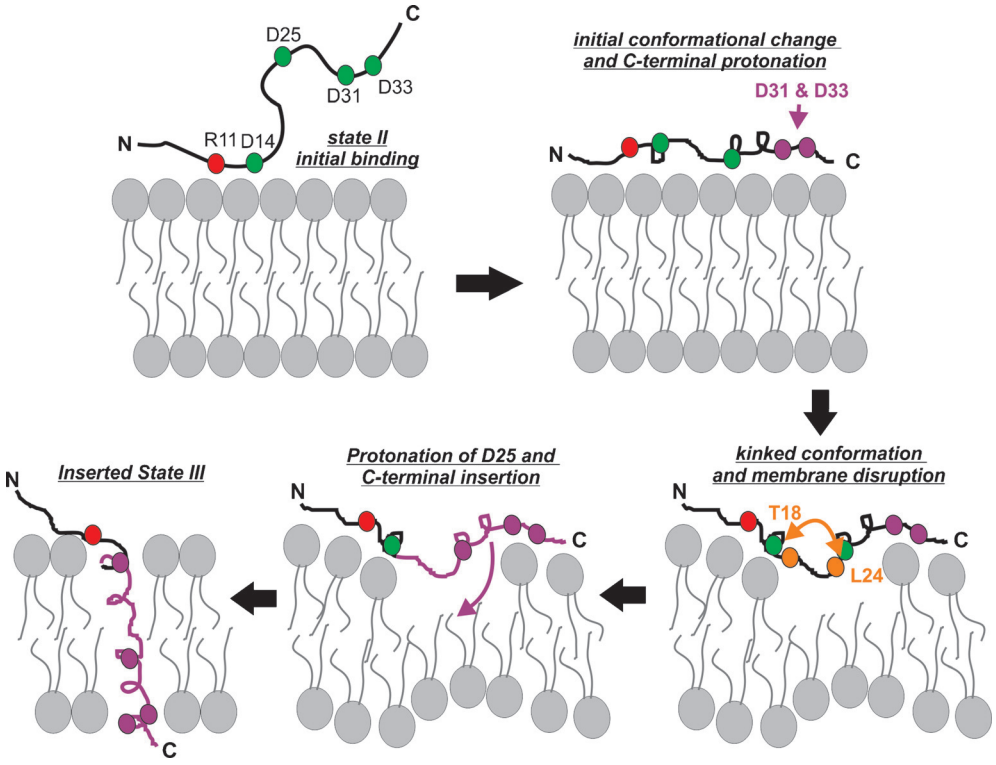

Figure 4. Proposed membrane insertion process of pHLIP at intermediate pH (green: negatively charged D residues, purple: protonated neutral D residues, orange: neutral T18/L24 residues, red: positively charged R11).

In summary, from data presented above we proposed the following additional details about the protonation-driven insertion process of pHLIP, as shown in Figure 4, set in the framework of previously established state II to state III transition.[1,4,11,33] At pH > 7.0, pHLIP initially adsorbs to membrane surface through N-terminal region interactions.[25] Protonations of C-terminal D/E residues at pH 6.4–7.0 promote the formation of a peripheral α-helix, which is embedded into the lipid head-group region and disturbs the membrane outer leaflet in a dynamic fashion. This helix is likely kinked at T19-P20, and the wedged conformation may be temporarily stabilized by side chain packings between T18 and L24. Perhaps with this wedged structure, and upon further protonations at D25 and D14, pHLIP sinks deeper into the membrane, eventually parting the lipids of the inner leaflet to reach full TM insertion. It is worth noting that our present mode is proposed based on experiments done with the single-component (i.e. POPC) liposome. Further investigations will be performed to confirm the proposal and to study the additional effects from more biologically relevant membrane components, especially the charged phospholipids that were reported to shift the local pH values at the water-bilayer interface.[38]

Acknowledgments

This work is supported by the start-up funding from SUNY-Binghamton Research Foundation and the National Science Foundation (MRI 0922815 and 1515028 to C.G.). We appreciate the helpful discussion with Dr. Lan Yao about the results.

Keywords: drug delivery · membranes · peptides · protonation · solid-state structures

How to cite: *Angew. Chem. Int. Ed.* **2016**, *55*, 12376–12381
Angew. Chem. **2016**, *128*, 12564–12569

[1] J. F. Hunt, P. Rath, K. J. Rothschild, D. M. Engelman, *Biochemistry* **1997**, *36*, 15177.
[2] L. Essen, R. Siegert, W. D. Lehmann, D. Oesterhelt, *Proc. Natl. Acad. Sci. USA* **1998**, *95*, 11673.
[3] H. Luecke, B. Schobert, H. T. Richter, J. P. Cartailler, J. K. Lanyi, *J. Mol. Biol.* **1999**, *291*, 899.
[4] Y. K. Reshetnyak, M. Segala, O. A. Andreev, D. M. Engelman, *Biophys. J.* **2007**, *93*, 2363.

[5] O. A. Andreev, A. D. Dupuy, M. Segala, S. Sandugu, D. A. Serra, C. O. Chichester, D. M. Engelman, Y. K. Reshetnyak, *Proc. Natl. Acad. Sci. USA* **2007**, *104*, 7893.
[6] A. G. Karabadzhak, D. Weerakkody, D. Wijesinghe, M. S. Thakur, D. M. Engelman, O. A. Andreev, V. S. Markin, Y. K. Reshetnyak, *Biophys. J.* **2012**, *102*, 1846.
[7] Y. K. Reshetnyak, O. A. Andreev, U. Lehnert, D. M. Engelman, *Proc. Natl. Acad. Sci. USA* **2006**, *103*, 6460.
[8] F. N. Barrera, J. Fendos, D. M. Engelman, *Proc. Natl. Acad. Sci. USA* **2012**, *109*, 14422.
[9] E. A. Sosunov, E. P. Anyukhovsky, A. A. Sosunov, A. Moshnikova, D. Wijesinghe, D. M. Engelman, Y. K. Reshetnyak, O. A. Andreev, *Proc. Natl. Acad. Sci. USA* **2013**, *110*, 82.
[10] N. Li, L. Yin, D. Thevenin, Y. Yamada, G. Limmon, J. Chen, V. T. Chow, D. M. Engelman, B. P. Engelward, *Future Microbiol.* **2013**, *8*, 257.
[11] O. A. Andreev, A. G. Karabadzhak, D. Weerakkody, G. O. Andreev, D. M. Engelman, Y. K. Reshetnyak, *Proc. Natl. Acad. Sci. USA* **2010**, *107*, 4081.
[12] M. An, D. Wijesinghe, O. A. Andreev, Y. K. Reshetnyak, D. M. Engelman, *Proc. Natl. Acad. Sci. USA* **2010**, *107*, 20246.
[13] D. Wijesinghe, D. M. Engelman, O. A. Andreev, Y. K. Reshetnyak, *Biochemistry* **2011**, *50*, 10215.
[14] A. Moshnikova, V. Moshnikova, O. A. Andreev, Y. K. Reshetnyak, *Biochemistry* **2013**, *52*, 1171.
[15] E. L. Sievers, P. D. Senter, *Annu. Rev. Med.* **2013**, *64*, 15.
[16] L. Yao, J. Daniels, D. Wijesinghe, O. A. Andreev, Y. K. Reshetnyak, *J. Controlled Release* **2013**, *167*, 228.
[17] C. J. Cheng, R. Bahal, I. A. Babar, Z. Pincus, F. Barrera, C. Liu, A. Svoronos, D. T. Braddock, P. M. Glazer, D. M. Engelman, W. M. Saltzman, F. J. Slack, *Nature* **2015**, *518*, 107.
[18] O. A. Andreev, D. M. Engelman, Y. K. Reshetnyak, *Front. Physiol.* **2014**, *5*, 97.
[19] K. E. Burns, M. K. Robinson, D. Thevenin, *Mol. Pharm.* **2015**, *12*, 1250.
[20] K. E. Burns, T. P. McCleerey, D. Thevenin, *Sci. Rep.* **2016**, *6*, 28465.
[21] J. O. Onyango, M. S. Chung, C.-H. Eng, L. M. Klees, R. Langenbacher, L. Yao, M. An, *Angew. Chem. Int. Ed.* **2015**, *54*, 3658; *Angew. Chem.* **2015**, *127*, 3729.
[22] M. Musial-Siwek, A. Karabadzhak, O. A. Andreev, Y. K. Reshetnyak, D. M. Engelman, *Biochim. Biophys. Acta Biomembr.* **2010**, *1798*, 1041.
[23] F. N. Barrera, D. Weerakkody, M. Anderson, O. A. Andreev, Y. K. Reshetnyak, D. M. Engelman, *J. Mol. Biol.* **2011**, *413*, 359.
[24] J. Fendos, F. N. Barrera, D. M. Engelman, *Biochemistry* **2013**, *52*, 4595.
[25] N. S. Shu, M. S. Chung, L. Yao, M. An, W. Qiang, *Nat. Commun.* **2015**, *6*, 7787.
[26] G. Platzer, M. Okon, L. P. McIntosh, *J. Biomol. NMR* **2014**, *60*, 109.
[27] K. Mitra, L. Ubarretxena-Belandia, T. Taguchi, G. Warren, D. M. Engelman, *Proc. Natl. Acad. Sci. USA* **2004**, *101*, 4083.
[28] R. Tycko, G. Dabbagh, *J. Am. Chem. Soc.* **1991**, *113*, 9444.
[29] G. A. Caputo, E. London, *Biochemistry* **2004**, *43*, 8794.
[30] M. Zoonens, Y. K. Reshetnyak, D. M. Engelman, *Biophys. J.* **2008**, *95*, 225.
[31] T. Lau, E. E. Ambroggio, D. J. Tew, R. Cappai, C. L. Masters, G. D. Fidelio, K. J. Barnham, F. Separovic, *J. Mol. Biol.* **2006**, *356*, 759.
[32] A. Drechsler, G. Anderluh, R. S. Norton, F. Separovic, *Biochim. Biophys. Acta Biomembr.* **2010**, *1798*, 244.
[33] Y. K. Reshetnyak, O. A. Andreev, M. Segala, V. S. Markin, D. M. Engelman, *Proc. Natl. Acad. Sci. USA* **2008**, *105*, 15340.
[34] D. Weerakkody, A. Moshnikova, M. S. Thakur, V. Moshnikova, J. Daniels, D. M. Engelman, O. A. Andreev, Y. K. Reshetnyak, *Proc. Natl. Acad. Sci. USA* **2013**, *110*, 5834.
[35] J. T. Vivian, P. R. Callis, *Biophys. J.* **2001**, *80*, 2093.
[36] C. R. Morcombe, V. Gaponenko, R. A. Byrd, K. W. Zilm, *J. Am. Chem. Soc.* **2004**, *126*, 7196.
[37] N. G. Sgourakis, W. M. Yau, W. Qiang, *Structure* **2015**, *23*, 216.
[38] A. Kundu, S. Yamaguchi, T. Tahara, *J. Phys. Chem. Lett.* **2014**, *5*, 762.

Received: May 27, 2016
Revised: July 22, 2016
Published online: August 31, 2016

